Investigation of the possible correlations between the structural, optical and magnetic traits of $Ni_xZn_{1-x}O$ nanoparticles fabricated via modified Pechini method

M. H. AHMADI[a*], ALI ABDOLAHZADEH ZIABARI[a,b]
[a]*Department of Optics and Laser, Faculty of Engineering, Lahijan Branch, Islamic Azad University, P.O. Box161, Lahijan, Iran*
[b]*Nano Research Lab, Lahijan Branch, Islamic Azad University, P.O. Box161, Lahijan, Iran*

Undoped and Ni-doped ZnO nanocrystalline powders were successfully synthesized by the sol–gel Pechini method. Analysis of the samples with X-ray diffraction showed that these nanopowders had a polycrystalline wurtzite structure. With Ni concentration increasing up to 10 Wt.%, all diffraction peaks corresponded to wurtzite structure of ZnO, but for $Zn_{0.9}Ni_{0.1}O$, secondary phase of NiO emerged. Based on the results of X-ray photoelectron spectroscopy (XPS), Ni incorporated into the ZnO lattice as Ni^{2+}. Scanning electron microscopy illustrated the formation of evenly distributed sphere like nano-clusters. UV-vis absorption results show that the band edge of ZnO nanoparticles is blue shifted with Ni doping concentration. The room temperature photoluminescence (PL) measurements illustrate UV emission around 390 nm (3.17 eV), which is ascribed to the near-band-edge (NBE) emissions of ZnO and broad green emission around 510 nm. The results of vibrating sample magnetometer (VSM) measurements showed that the low and heavy doped ZnO nanoparticles have more diamagnetic features while the moderate doped sample possesses good ferromagnetic characteristics.

(Received February 5, 2015; accepted March 19, 2015)

Keywords: Nanopowder, Pechini method, XPS, Optical properties, Magnetic properties

1. Introduction

Recently, semiconductor nanostructures have attracted extraordinary attention due to their unique physical and chemical properties, which make them as the ideal advanced functional materials for nanodevices [1, 2]. As an outstanding metal oxide, ZnO continues to catch attention for its privileged functional properties for various applications such as transparent conducting oxides, ultra-violet lasers, light modulators, anti reflective coatings, mechanical actuators, displays and solar panels [2, 3]. Ferromagnetism above room temperature in dilute magnetic semiconductors (DMSs) such as transition metal doped ZnO continues to be intense because of promising application for advanced spintronics devices [3]. ZnO is a II–VI compound semiconductor, has a wide band gap of 3.37 eV and a large exciton binding energy of 60 meV at room temperature [4]. Combining the excellent optical properties with room-temperature ferromagnetism, many magnetic–optic devices could be made from ZnO-based DMSs. Among the thermoelectric oxides, zinc oxide presents a large Seebeck coefficient and a high thermal stability [5]. Due to its privileged conducting properties, ZnO has also been investigated as a transparent conducting and piezoelectric material [6-8].

Compared to undoped semiconductors, doped materials offer the possibility of using the dopant to tune their electronic, magnetic and optical properties. Also, the incorporation of dopants can sometimes lead to development of some unique properties useful for fabrication of devices. Over the past few years, ZnO have been successfully doped with different impurities such as Al, Mn, Fe, Cd, Co and Cu [9-13]. In recent years, numerous efforts have been concentrated on studying transition metal-doped ZnO nanostructures due to their potential use in producing nanoscale spintronic devices [2, 3 and 14]. Amongst them, Ni is the most efficient doping elements to improve and tune the optical, electrical and magnetic properties of ZnO [15-18]. Ni is also very much unstable metal in the ZnO matrix; hence it has the tendency to form clusters of metallic Ni or NiO [15]. In DMSs, Ni can successfully replace Zn site and the exchange interaction induces the room temperature ferromagnetism that finds its application in spintronics [19, 20, and 21]. During the past several years, nanomaterial have been prepared using different methods, including chemical solution deposition [2], sol–gel [22], pyrohydrolysis route [23], wet-chemical techniques [24], etc. In comparison with other oxide fabrication methods, the polymerized complex process initiated by Pechini is a low temperature synthesis route which can produce a more uniform particle distribution [25]. In the present study, to lessen the hydrolysis and gelation time, polymeric precursors were prepared using zinc acetate and a mixed solution of citric acid and ethylene glycol as a chelating agent and reaction medium, respectively. ZnO nanopowders were then prepared by the mentioned modified Pechini method and the influence of Ni doping on the pertinent crystal phase and morphology was investigated precisely. Furthermore, the optical,

photoluminescence and magnetic traits of fabricated nanoparticles were evaluated and discussed phenomenologically.

2. Experimental details

2.1. Synthesis

$Ni_xZn_{1-x}O$ (x =0.00, 0.05 and 0.10) nanopowders were prepared by the sol–gel Pechini method. The process is based on metallic citrate polymerization by using of ethylene glycol. A hydrocarboxylic acid, such as citric acid, is used to chelate cations in an aqueous solution. The addition of ethylene glycol leads to the formation of an organic ester. Polymerizations promoted by heating the mixture, results in a homogeneous resin in which metal ions are uniformly distributed throughout the organic matrix. Zinc nitrate [$Zn(NO_3)_2{\cdot}6H2O$] and nickel sulphate [$Ni(SO_4)_2.H_2O$] powders were chosen as starting materials. Two separate solutions were prepared by dissolving measured amount of zinc nitrate and citric acid into 25ml of ethylene glycol and deionized water, respectively. The concentration of as-prepared solutions was chosen to be 0.4M. After complete dissolution of the precursors, citric acid solution was added to zinc nitrate solution and then chelated in with magnetic stirring at 80 ^oC. After 30 min, nickel sulphate was added to the solution. The Ni/Zn ratio in the solution was changed as 0, 5% and 10%. The resulting mixture was stirred for 4 hours at 80 °C in air to yield a transparent and homogeneous solution. Afterwards, the prepared sol was slowly cooled in air down to room temperature and then aged for 24 h in that situation. Eventually, the sol was put into a tube furnace and annealed in air at 500 ˚C for 2 h.

2.2. Characterization

The structure of the prepared nanopowders was studied by the X-ray diffraction (XRD) method using a XRD6000, Shimadzu System with Cu K_α radiation (λ= 0.15418 nm). Surface morphology of the powders was studied by scanning electron microscopy (SEM) (LEO, 1430VP with 15 kV accelerating voltage). Quantitative analyses were conducted by energy-dispersive X-ray analysis (EDX; LEO 1430VP) with an accelerating voltage of 17 kV. The absorbance spectra of the powders were measured using a Shimadzu (UV-3101PC) spectrophotometer. The low-temperature PL measurements were recorded using a Perkin-Elmer LS-5 luminescence spectrometer. The magnetic properties of the powder samples were performed by MDK 6 VSM vibrating sample magnetometer (VSM).

3. Results and discussion

3.1. Structural, compositional and morphological studies

The X-ray diffraction patterns for pure and Ni doped ZnO nanopowders are shown in Fig.1. All diffraction peaks in pure sample can be indexed to ZnO hexagonal wurtzite structure (JCPDS No. 36-1451). Besides, no extra diffraction peak from Ni-related second phase was observed for 5% doped sample. This trend has been reported for low-nickel-content doped ZnO powders [8, 26, and 27] and may be attributed to the incorporation of Ni ion into the Zn lattice site. On the other hand, for 10% doped sample a new diffraction peak appeared on (200) plane that can be identified either to NiO or to Zn_yNi_zO with cubic structure [5]. Formation of NiO secondary phase can be attributed to the limited solid solubility of Ni in ZnO host matrix [15]. As it is evident from the figures, NiO peak intensity increases with Ni concentration. At the same time, the intensity of the characteristic peaks for ZnO decreases whiles the affiliated full-width at half-maximum (FWHM) increases with Ni content. This can be associated with the presence of nickel–zinc compounds in the amorphous phase and with a diminishing of the zinc oxide grain size [28]. The crystallite size of the samples was calculated by Scherrer's formula [29]

$$D = \frac{k\lambda}{\beta \cos\theta} \qquad (1)$$

where D is the crystallite size, β is the broadening of diffraction line measured at half of its maximum intensity and λ is the incident X-ray wavelength. After introducing Ni, the crystallinity was deteriorated and the grain size also decreased from 19 to 15 nm. It might be owing to lower ionic radius of Ni^{2+} (69Å) compared with Zn^{2+} (74Å).

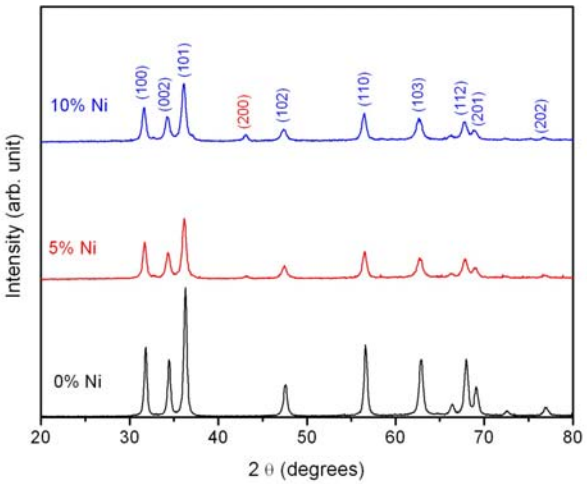

Fig.1. XRD patterns of undoped, 5Wt% and 10Wt% Ni doped ZnO nanopowders.

The ratio of Ni and Zn in the doped nanopowders is investigated by the EDX measurement under the plan detection mode. The penetrated depth of focused high energy electrons into the ZnO:Ni sample is about 2 μm. The results in Fig. 2 confirm the presence of Zn and Ni, with Ni/Zn weight percentages of 5.23/48.94 and 11.49/49.03 for 5% and 10% doped samples, respectively.

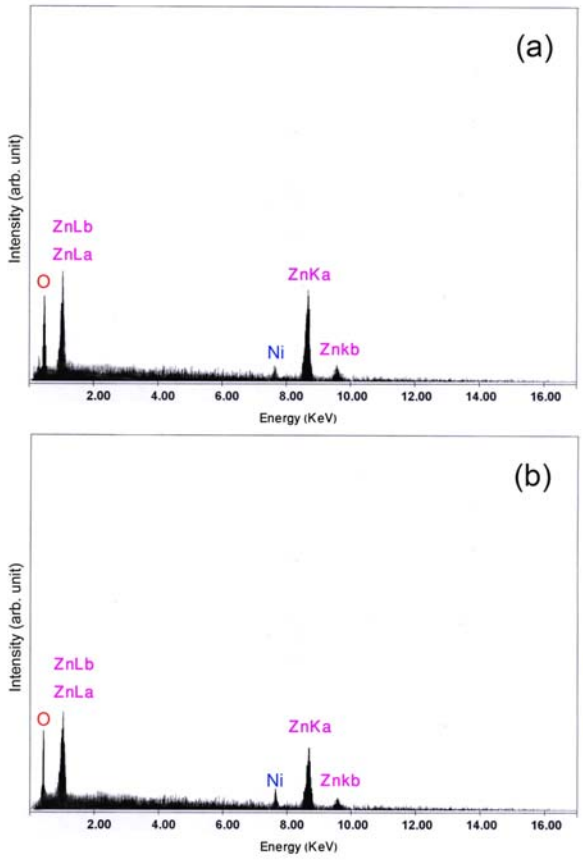

Fig. 2. EDX spectra for ZnO:Ni nanopowders with different Ni concentration:(a) 5Wt% and (b) 10Wt%.

Scanning electron microscopy (SEM) is a convenient technique to study the surface morphology of nanostructures. Fig. 3 shows the SEM images of the pure and Ni doped ZnO nanopowders prepared by sol–gel Pechini method. Undoped ZnO nanopowders exhibit spherical shape and some agglomerations are seen in the background. In the meantime, the cluster size indicates high sensitivity to the nickel concentration. As Ni content rises from 0 to 10wt%, the cluster size decreases tardily that confirms the XRD results.

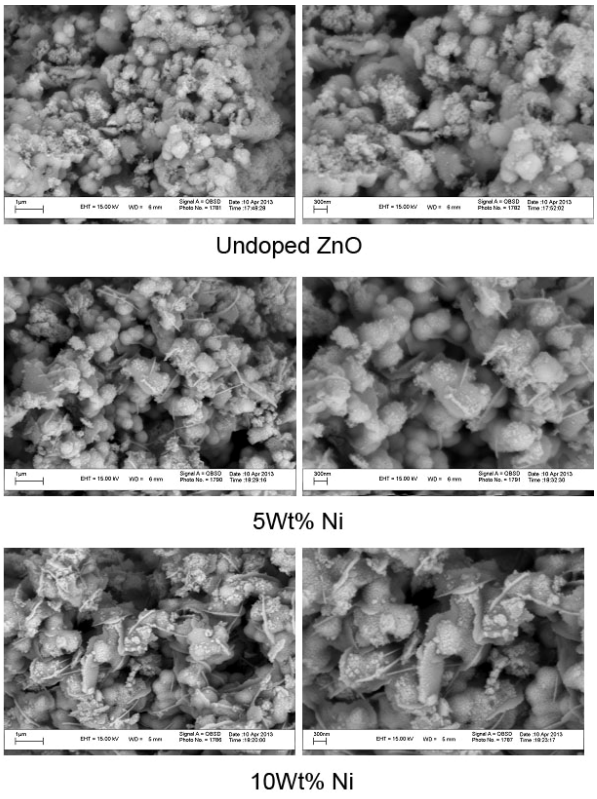

Fig. 3. SEM micrographs of undoped, 5 Wt% and 10 Wt% Ni-doped ZnO nanopowders.

3.2. Optical properties

Optical absorption spectroscopy and photoluminescence measurements provide precious information on the optoelectronic features of semiconductors [30]. To study the electronic interactions near the band gap region due to doping of Ni, UV–visible absorbance measurements were undertaken (Fig. 4). The change in absorption peak due to doping indicates a change in the band structure. It is observed that absorption edges of ZnO:Ni are at 373.15, 372.21 and 366.25 nm for 0, 5 and 10Wt% doped samples, respectively. The position of the absorption edge is observed to shift toward lower wavelength side with increase in Ni concentration in ZnO, indicating an increase in the band gap with Ni doping. This blueshift behavior can in principle be explained by the Moss–Burstein band filling effect, which is frequently observed in n-type semiconductors [31, 32]. Similar result is reported in the literature [33].

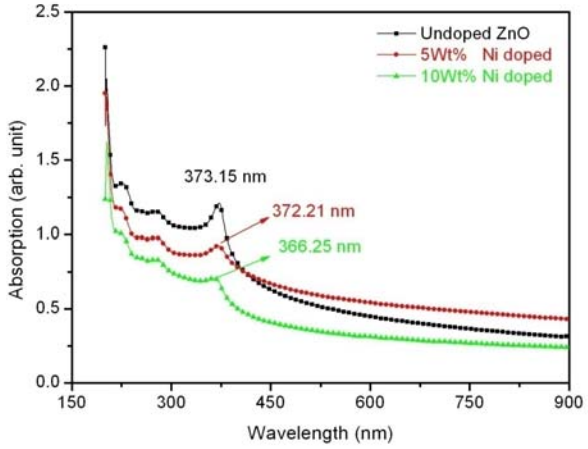

Fig. 4. Absorption spectra for undoped and Ni-doped ZnO nanopowders.

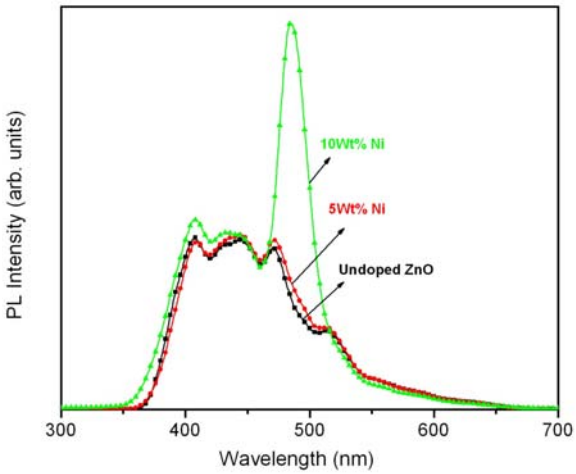

Fig. 5. Room temperature PL spectra for undoped and Ni-doped ZnO nanopowders.

3.3. Photoluminescence studies

The effects of Ni-doping on optical emission and defect formation were investigated by PL measurements. Room temperature PL emission spectra for undoped and Ni-doped ZnO nanopowders are shown in Fig. 5. As seen from the figure, undoped and 5Wt. % Ni-doped ZnO exhibit two emission peaks, a broad one in the range of 360-480 nm and another weak one around 520 nm.

For 10Wt. % Ni-doped sample, the spectrum conforms to the mentioned spectra from 360 to 460 nm but then rises abruptly. The above mentioned broad emission at 360–480 nm is too wide to be associated to only one defect or impurity, so it should be deconvoluted. To do that, the PL spectra of undoped and Ni-doped ZnO are analyzed by a Lorentzian curve fitting as shown in Fig. 6.The results of the peak fit show that the spectral band consisting of violet, blue and green regions. Notably, there is no significant shift in PL peaks observed due to Ni doping in ZnO.

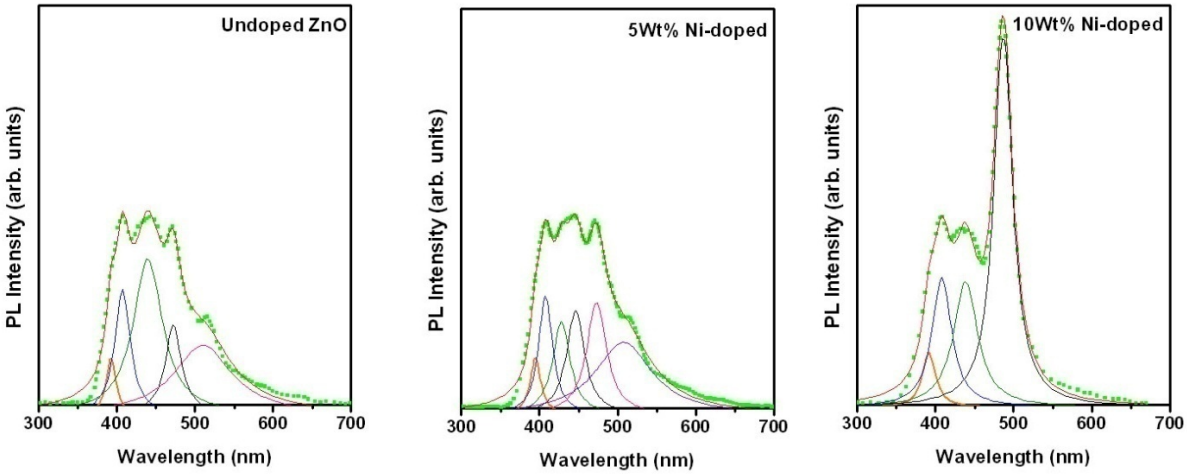

Fig. 6. Multiple Lorentzian fittings of the room temperature PL spectra for undoped and Ni-doped ZnO nanopowders.

The violet emission band is convoluted into two peaks; the weak violet luminescence peak located at ~380 nm, corresponding to a photon energy of ~3.26 eV, is related to near band edge emission. Another one component centered at ~407 nm (3.05eV) is usually ascribed to the recombination of an electron from zinc interstitial (Zn_i./Zn_i..) and a hole in the valence band [34]. Other peaks are found in the visible blue spectral region via the fitting of the entire emission peaks, which may correspond to zinc vacancy (V_{Zn}) and interstitial zinc (Zn_i), respectively, that are in good agreement with other studies in the literature [35, 36]. A weak green emission peak is observed in ~520 nm (2.38 eV) for undoped and 5Wt. % Ni-doped samples while a strong blue-green emission was

found around 490 nm (2.53 eV) for 10 Wt. % Ni-doped sample. Vanheusden et al. argued that singly ionized oxygen vacancies are responsible for the green luminescence in ZnO [37]. The origin of blue-green luminescence peak at ~490 nm is related to the defect levels introduced due to substitution of Ni^{2+} in the Zn^{2+} site by doping. This result is in conformity with the result obtained by Gayen et al [38]. Since d–d transitions in NiO are dipole-forbidden by the Laporte selection rule [39], it would be difficult to observe PL spectra from NiO. The strengthening of the ZnO blue-green luminescence with increasing Ni^{2+} concentration demonstrates that the energy transfer from ZnO to Ni^{2+} is more efficient than that to the defect states in ZnO. According to Förster's theory [40], the energy transfer rate is proportional to the spectral overlap, and inversely proportional to the distance (D) between the two sites. In this study, for samples doped with different concentration of Ni^{2+}, D would decrease with increasing Ni^{2+} concentration, leading to the enhancing of the energy transfer rate.

3.4. XPS study

The composition and chemical state of the elements present in Ni-doped ZnO nanoparticles were studied using XPS measurement. Fig.7 shows the survey XPS spectrum for 5Wt. % Ni-doped ZnO nanopowder.

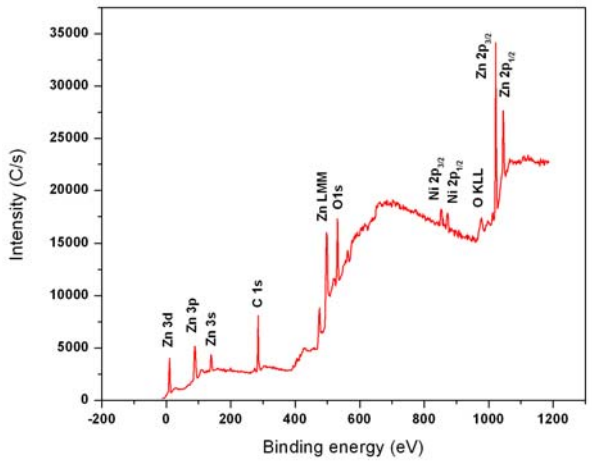

Fig. 7. Typical XPS survey spectrum for Ni-doped ZnO nanoparticles (5 Wt.% Ni).

The spectrum showed all the peaks related to Zn, O and Ni elements present in the sample in addition to C. Fig. 8 depicts the Zn $2p_{3/2}$ and Zn $2p_{1/2}$. The result is in good agreement with the reported values [41], which indicate +2 state of Zn in the nanopowder.

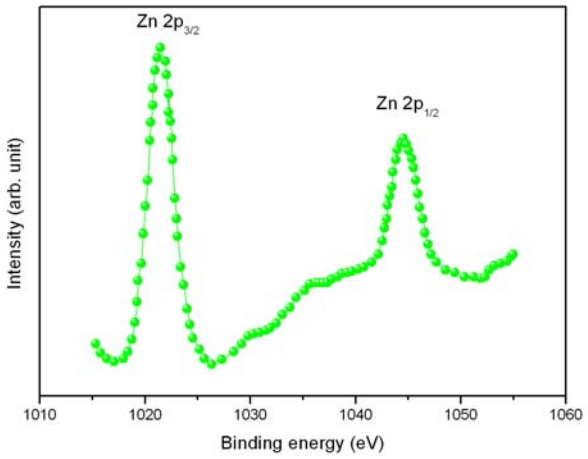

Fig. 8. Zn 2p core level spectra for 5 Wt.% Ni-doped ZnO nanopowder.

Besides, Fig.9 shows Ni $2p_{3/2}$ peak of the 5Wt. % Ni-doped ZnO nanopowder that indicates an evident satellite structure around 860 eV. Similar peak structure was observed for nickel oxides and is linked to O(2p)→Ni(3d) charge-transfer transition or hybridization [41, 42]. On the other hand, the Ni $2p_{3/2}$ peak is located at a binding energy around 854.13 eV, which is different from the binding energy value of metallic Ni (852.7 eV) or Ni^{+2} in NiO (853.5 eV) or Ni^{+3} in Ni_2O_3 (857.3 eV) [43]. This implies that nickel is in +2 valence state in the prepared powder. Hence, it is possible that there is a replacement of Zn^{+2} by Ni^{+2} in the ZnO lattice.

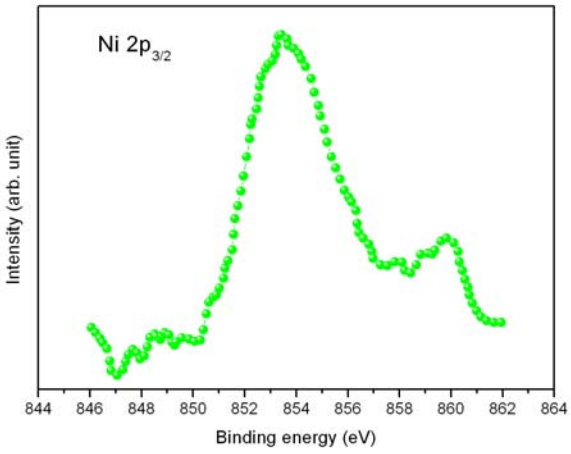

Fig. 9. Ni $2p_{3/2}$ core level spectra for 5 Wt.% Ni-doped ZnO nanopowder.

3.5. Magnetic properties

In order to understand the magnetic behavior of the undoped and Ni-doped ZnO nanopowders, the magnetization versus field dependence curves of these samples were measured at 300K and are shown in Fig. 10. The maximum applied field was 8 kOe. Undoped ZnO nanopowder did not exhibit ferromagnetic behavior at room temperature (it is not shown). Similar behavior has been reported frequently for undoped ZnO by the others [15, 44].

On the other hand, Ni-doped samples exhibit clear ferromagnetic behavior at room temperature. The observed ferromagnetic behavior of 5 and 10 Wt. % Ni-doped ZnO samples can be ascribed to the Ni ions substituting for Zn lattice ions [15]. The loops show remanence ratio (M_r) of 0.48×10^{-3} and 0.13×10^{-3} emu/cm^2 and coercivity (H_c) of 161 and 131Oe for 5 and 10 Wt. % Ni-doped samples, respectively. The decline of ferromagnetism can be linked to the emerging of NiO phase. It has been reported that NiO shows antiferromagnetic effects [43]. The antiferromagnetic interaction between neighboring Ni–Ni ions suppressed the ferromagnetism at higher doping concentration of Ni, leading to the decrease of the ferromagnetism.

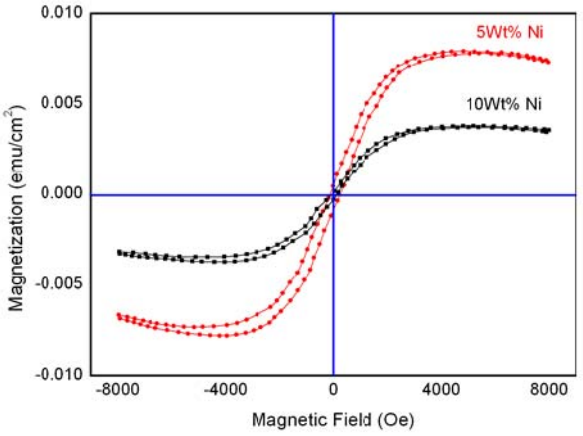

Fig.10. Room temperature M–H curves of 5 and 10 Wt. % Ni-doped ZnO nanopaticles.

4. Conclusion

In summary, nickel doped ZnO semiconductor nanoparticles are prepared by the sol-gel Pechini method. XRD analysis study showed wurtzite structures for all prepared nanocrystals. The calculated particle sizes were between 15 nm and 19 nm. The quantitative analysis of the samples was carried out by using energy dispersive X-ray (EDX) analysis to study the stoichiometry of the nanopowders. SEM results showed the spherical shaped agglomerations of the prepared nanopowders. Optical studies indicated that the band gap of Ni-doped ZnO nanopowders increases with Ni content. Meanwhile, PL emission intensity was found to be greatly dependent on Ni concentration. Magnetic measurements indicated that Ni-doped ZnO samples show clear ferromagnetic behavior at room temperature and the ferromagnetism was decreased with high level doping of nickel.

Acknowledgment

This study was supported by the research fund of Islamic Azad University, Lahijan Branch, Iran. The authors are grateful to Dr. M. Houshiar for kindly assistance in UV, PL and VSM analysis. The authors also thank a lot Mr. Reza Refahati, Mr. H.A. Kazempour and Mr. M. Sirous for all of their selfless cooperation.

References

[1] R.M. Mohamed, M.A. Al-Rayyani, E.S. Baeissa, I.A. Mkhalid, Journal of Alloys and Compounds **509**, 6824 (2011).
[2] A. Abdolahzadeh Ziabari, S.M. Rozati, Physica B **407,** 4512 (2012).
[3] Peng Hua, Ning Hana, Dangwen Zhanga, Johnny C. Hob, Yunfa Chen, Sensors and Actuators B **169**, 74 (2012).
[4] S.H. Chiu, J.C.A. Huang, Journal of Non-Crystalline Solids **358**, 2453 (2012).
[5] H. Colder, E. Guilmeau, C. Harnois, S. Marinel, R. Retoux, E. Savary, Journal of the European Ceramic Society **31,** 2957 (2011).
[6] T. Al-Harbi, Journal of Alloys and Compounds **509**, 387 (2011).
[7] J. Zhao, L. Wang , X. Yan, Y. Yang, Y. Lei, J. Zhou, Y. Huang, Y. Gu, Y. Zhang, Materials Research Bulletin **46,** 1207 (2011).
[8] X. Wang, M. Zhao, FangLiu, J. Jia, X. Li, L. Cao, Ceramics International **39**, 2883 (2013).
[9] K.J. Chen, T.H. Fang, F.Y. Hung, L.W. Ji, S.J. Chang S.J. Young , Y.J. Hsiao, Applied Surface Science **254,** 5791 (2008).
[10] S. Mondal, S.R. Bhattacharyya, P. Mitra, Bull. Mater. Sci., **36**(2), 223 (2013).
[11] J. Wang, J. Wan, K. Chen, Materials Letters **64**, 2373 (2010).
[12] A. Abdolahzadeh Ziabari, F.E. Ghodsi, Thin Solid Films **520**, 1228 (2011).
[13] H. Xu, Q. Zhao, H. Yang, Y. Chen, J Nanopart Res **11**, 615 (2009).
[14] G. Murugadoss, J. Mater. Sci. Technol. **28**(7), 587 (2012).
[15] S. Yılmaz, E. McGlynn , E. Bacaksız, J. Cullen, R.K. Chellappan, Chemical Physics Letters **525–526**, 72 (2012).
[16] X. Zhao, E. Liu, R.V. Ramanujan, J. Chen, Current Applied Physics **12**, 834 (2012).
[17] D.J. Qiua, H.Z. Wua, A.M. Feng, Y.F. Lao, N.B. Chen, T.N. Xu, Applied Surface Science **222**, 263 (2004).

[18] G. J. Huang, J. B. Wang, X. L. Zhong ,G. C. Zhou, H. L. Yan, J Mater Sci. **42**, 6464 (2007).
[19] J.J. Lu, T.C.Lin , S.Y.Tsai , T.S.Mo, K.J.Gan, Journal of Magnetism and Magnetic Materials **323**, 829 (2011).
[20] S.H. Chiu, J.C.A. Huang, Journal of Non-Crystalline Solids **358,** 2453 (2012).
[21] R. Saravanan, Kalavathy Santhi, N. Sivakumar, V. Narayanan, A. Stephen, Materials Characterization **67**, 10 (2012).
[22] A. Abdolahzadeh Ziabari, F.E. Ghodsi, J. Alloys Compd. **509**, 8748 (2011).
[23] I. Ganesh, P.S. Chandra Sekhar, G. Padmanabham, G. Sundararajan, Applied Surface Science **259**, 524 (2012).
[24] R. Ullah, J. Dutta, Journal of Hazardous Materials **156**, 194 (2008).
[25] M.I.B. Bernardi, L.E. Soledade, I.A. Santos, E.R. Leite, E. Longo, J.A. Varela, Thin Solid Films **405**, 228 (2002).
[26] X. Chu, X. Zhu, Y. Dong, T. Chen, M. Ye, W. Sun, Journal of Electroanalytical Chemistry **676**, 20 (2012).
[27] R.K. Singhal , Sudhish Kumar , Y.T. Xing, U.P. Deshpande , T. Shripathi, S.N. Dolia, E. Saitovitch, Materials Letters **65**, 1485 (2011).
[28] M.A. Flores, R.Castanedo, G.Torres, O.Zelay, Solar Energy Materials & Solar Cells **93**, 28 (2009).
[29] B.D. Cullity, S.R. Stock, Elements of X-ray Diffraction, Prentice Hall, New Jersey (2001) 167.
[30] A. Abdolahzadeh Ziabari, F.E. Ghodsi, Journal of Luminescence **141**, 121 (2013).
[31] A. Abdolahzadeh Ziabari, F.E. Ghodsi, Acta Physica Polonica A **120**(3) 536 (2011).
[32] A. Abdolahzadeh Ziabari, F.E. Ghodsi, G. Kiriakidis, Surface and Coating Technology **213**, 15 (2012).
[33] J. Zhao, L. Wang, X. Yan, Y. Yang, Y. Lei, J. Zhou, Y. Huang, Y. Gu, Y. Zhang, Materials Research Bulletin **46** 1207 (2011).
[34] R. Rajalakshmi, S. Angappane, Materials Science and Engineering B **178**, 1068 (2013).
[35] H. Liu, X. Zhang, L. Li, Y.X. Wang, K.H. Gao, Z.Q. Li, R.K. Zheng, S.P. Ringer, B. Zhang, X.X. Zhang, Appl. Phys. Lett. **91**, 072511 (2007).
[36] X. Zhang, W. H. Wang, L. Y. Li, Y. H. Cheng, X. G. Luo, H. Liu, Z. Q. Li, R. K. Zheng, S. P. Ringer, EPL **84,** 27005 (2008).
[37] K. Vanheusden, W. Warren, C. Seager, D. Tallant, J. Voigt, B. Gnade, Journal of Applied Physics **79**, 7983 (1996).
[38] R.N. Gayen, A. Rajaram, R. Bhar, A.K. Pal, Thin Solid Films **518**(6), 1627 (2010).
[39] V.V. Volkov, Z. Wang, B. Zou, Chemical Physics Letters **337**, 117 (2001).
[40] G. Allan, C. Delerue, Phys. Rev. B **75**, 195311 (2007).
[41] S. Ghosh, P. Srivastava, B. Pandey, M. Saurav, P. Bharadwaj, D.K. Avasthi, D. Kabiraj, S.M. Shivaprasad, Appl. Phys. A **90**, 765 (2008).
[42] S. Hüfner, G.K.Wertheim, Phys. Rev. B **8**, 4857 (1973).
[43] G. H. Yu, L. R. Zeng, F. W. Zhu, C. L. Chai, W. Y. Lai, J. Appl. Phys. **90**(8), 4039 (2001).
[44] D.A. Schwartz, K.R. Kittilatved, D.R.Gamelin, Appl. Phys. Lett. **85**, 1395 (2004).

*Corresponding author: mh.ahmadi24@yahoo.com